Int J Adv Manuf Technol (2018) 94:4115–4123
DOI 10.1007/s00170-017-1129-9

ORIGINAL ARTICLE

Prediction of surface topography in precision hard machining based on modelling of the generation mechanisms resulting from a variable feed rate

W. Grzesik [1]

Received: 10 May 2017 / Accepted: 13 September 2017 / Published online: 29 September 2017

Abstract The paper presents an original contribution to the prediction of surface topography produced by precision hard turning operations using CBN cutting tools and the variable feed rate of 0.025–0.075 mm/rev. The differences between theoretical and real surface roughness parameters *Rz* and *Sz* are quantified in terms of springback effect, additional smoothing of irregularities and side flow effect. The primary experimental study includes measurements of 2D and 3D surface roughness parameters using contact profilometer. Correspondingly, cutting forces were measured using a piezoelectric dynamometer, and based on this data, specific corresponding values of ploughing energy and friction coefficient were determined. It was found that the measured value of maximum height of the surface *Sz* differs from the theoretical value mainly due to elastic recovery of the machined surface and the smoothing effect at the lower feeds and the elastic recovery and the side flow effect at the higher feeds employed. An empirical model for the prediction of the Sz value in function of the feed rate is derived. The prediction accuracy can be improved by advanced numerical modelling of surface generation mechanisms and associated distortions.

Keywords Hard turning · Friction · Springback effect · Side flow effect · Surface roughness

✉ W. Grzesik
w.grzesik@po.opole.pl

[1] Faculty of Mechanical Engineering, Opole University of Technology, 45-271 Opole, Poland

1 Introduction

Hard machining has been established as a leading machining technology for various machine components made of high-strength steels with surface finish comparable to grinding effects [1]. Predominantly, scientific and engineering issues of hard turning do not address sufficiently surface topography and surface assessment is narrowed to the *Ra* or *Rz* roughness parameters [1, 2]. In addition, the distortion of surface topography in finish hard machining has not been investigated satisfactorily. It should be noted that surface generation mechanisms developed for machining of materials of low and medium hardness cannot be applied for hard materials. This is due to the fact that strong adhesive interaction between the chip and the tool material characteristic for severe plastic deformation does not occur in hard machining [1]. The molecular-mechanical theory of friction was applied for predicting the transition from interfacial sliding to micro-cutting when turning AISI 1045 steel with P10 carbide cutting tools [3]. Instead, intensive ploughing action of the cutting edge and resulting elastic recovery of the hard-machined layer are predominantly observed when removing material using CBN cutting tools with high negative rake angles. It is evident to incorporate the specific influence of the mechanics of the chip formation and the tool wear in the formation of the machined surface and subsurface layer. It was revealed [4] that in ultraprecision hard turning, the generation of surface roughness is limited by such factors as tool cutting edge defects, cutting vibration and elastic and plastic deformation of the workpiece material. Plastic deformation becomes an important component when the feed decreases down to 0.02 mm/rev (20 μm/rev) (percentage about 90%). Moreover [5], the relation between measured and theoretical values of P-V (*Rz*) parameter for turning and facing of aluminium with cemented carbide and PCD tools suggests that the *Rz* values down to 0.02 times the insert edge

radii are possible. Modelling of material side flow for CBN tools in hard turning of AISI 52100 bearing steel with variable feed rate (f = 0.1, 0.2 and 0.4 mm/rev) and nose radius (r_ε = 0.4, 1.2, 1.6 and 3.4 mm) indicated that it increases from about 1 μm up to about 12 μm for the tool nose radius r_ε = 0.4 and 3.4 mm, respectively [6]. The side flow effect was also investigated along with 3D surface topography for high-speed hard turning of a bearing steel of 60 ± 2HRC with the cutting speed of 100–300 m/min and feed rate of 0.05 and 0.1 mm/rev [7]. It is reasoned that 3D roughness parameters better characterize the deterioration of the machined surface due to flank wear and side flow is intensified at higher speeds. Similarly, the springback effect (elastic recovery) was predicted under variable cutting speed of 10–450 m/min using FEM for aluminium and titanium [8]. For instance, it increases from about 3 up to 10 μm for Ti6Al4V alloy when cutting speed increases from 10 to 100 m/min. A high coherence between *Ra* parameter and the springback was found.

The prediction of the surface roughness produced by machining operations is based on the machining theory, experimental investigations, designed experiments, artificial intelligence (AI) and multi-scale analysis [9, 10]. Geometrical, physical, empirical and simulation models are the mostly used ones [2, 9]. In empirical models, the most important variables are the feed rate, the tool corner radius, the depth of cut and the cutting speed in that order. The practical value of empirical models is substantially limited to the set of variable factors selected by manufacturers and, as a result, they used simple theoretical formulas for both *Ra* and *Rz* roughness parameters and compare them with measured values [2]. The main drawback of such approach was that all associated effects leading to the distortion of surface topography (for instance Brammertz's model represented by Eq. 8) are considered individually. The author's analysis suggests that they occur together and their intensity depends on the cutting parameters and the real geometry of cutting tools used. The main advantage of this study is that several factors such as ploughing action of the cutting edge, elastic recovery, smoothing effect of the increased irregularities and unremoved material on the surface were considered comprehensively in precision hard turning (PHT) with variable feed of 0.025–0.075(0.1) mm/rev using chamfered CBN tools. The selection of the feed rate lower than 0.1 mm/rev results from the fact that its increase above 0.1 mm/rev causes a rapid increase of the *Ra* roughness parameter [11].

2 Measurements and computations of process data

2.1 Measurements of cutting forces and specific energies

Measurements of three components of the resultant cutting force (F_c, F_f and F_p) were performed in the *xyz* coordinate system as shown in Fig. 1a. These three cutting forces were transformed into the l_{mn} coordinate system (Fig. 1 b) using two transformation matrixes given by Eq. 1 [12] in order to determine the friction coefficient for the rake face. The geometrical details of the machined layer generated by means of rounded nose inserts is shown in Fig. 1a.

According to Fig. 1, the l_{mn} system is obtained by rotating the *xyz* system by the inclination angle λ_s around the *x*-axis and by the normal rake angle γ_n around the *y*-axis. The product of relevant transformation matrixes $[TM]_x$ and $[TM]_y$ is defined by Eq. 1.

$$\begin{aligned}[TM] &= [TM]_x[TM]_y \\ &= \begin{bmatrix} 1 & 0 & 0 \\ 0 & \cos\lambda_s & -\sin\lambda_s \\ 0 & \sin\lambda_s & \cos\lambda_s \end{bmatrix} \begin{bmatrix} \cos\gamma_n & 0 & -\sin\gamma_n \\ 0 & 1 & 0 \\ \sin\gamma_n & 0 & \cos\gamma_n \end{bmatrix} \\ &= \begin{bmatrix} \cos\gamma_n & 0 & -\sin\gamma_n \\ -\sin\lambda_s\sin\gamma_n & \cos\lambda_s & -\sin\lambda_s\cos\gamma_n \\ \cos\lambda_s\sin\gamma_o & \sin\lambda_s & \cos\lambda_s\cos\gamma_n \end{bmatrix} \end{aligned} \quad (1)$$

Hence, the transformation of force components from the *xyz* coordinate system to the l_{mn} system using the matrix [TM] is given by Eq. 2.

$$\begin{bmatrix} F_n \\ F_l \\ F_m \end{bmatrix} = [TM] \begin{bmatrix} F_x \\ F_y \\ F_z \end{bmatrix} \quad (2)$$

By multiplying symmetrical 3 × 3 matrix (Eq. 1) and column matrix in Eq. 2, one obtains three equations for determining F_l, F_m and F_n forces in terms of the measured F_x, F_y and F_z forces. They are as follows:

$$F_l = -F_x\sin\lambda_s\sin\gamma_n + F_y\cos\lambda_s - F_z\sin\lambda_s\cos\gamma_n \quad (3.1)$$

$$F_m = F_x\cos\lambda_s\sin\gamma_n + F_y\sin\lambda_s + F_z\cos\lambda_s\cos\gamma_n \quad (3.2)$$

$$F_n = F_x\cos\gamma_n - F_z\sin\gamma_n \quad (3.3)$$

Specific cutting k_c and ploughing k_p pressures are calculated based on the equivalent cutting edge of the length l_k and the mean uncut thickness (UCT) h_m shown in Fig. 1 a. Hence:

$$k_c = F_c \Big/ A_c \quad (4a)$$

$$k_p = F_p \Big/ A_c \quad (4b)$$

where the cross-sectional area of cut $A_c = h_m \times l_k$.

Values of the specific cutting e_c and ploughing e_p energies are determined by the transformation of units from N/mm^2 (10^6 × N/m^2) to 10^6 × N × m/m^2 × m = MJ/m^3. Finally, the unit of the specific cutting energy was GJ/m^3 (10^3 × MJ/m^3).

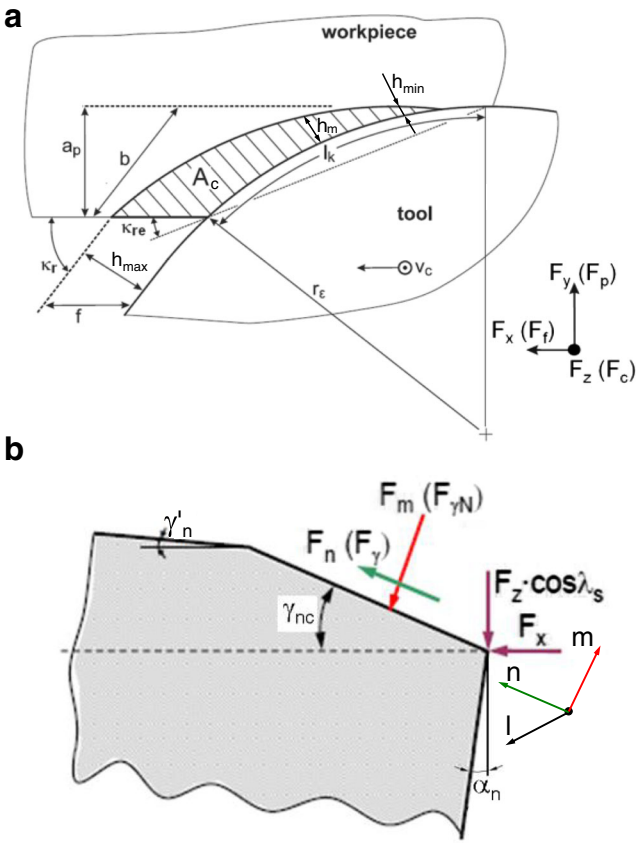

Fig. 1 Dimensioning of uncut chip (**a**) and resolution of resultant cutting force in l_{mn} coordinate system (**b**) [12, 13]

2.2 Measurements of surface roughness parameters

Surface topographies generated by CBN tools were measured by means of the stylus contact method using a TOPO-01P contact profilometer and three non-contact methods: confocal, white-light scanning interferometer and optical with focus variation using versatile S-lynx 3D profiler by Sensofar Metrology, because the contact profilometer is not equipped with the function of precise contour shape measurement. The approximation of the cutting edge radius was performed automatically using a set of reference circles.

3D roughness parameters were determined according to ISO 25178 standard, and surface topographies were visualized using a Digital Surf, Mountains® Map package. They include S and V standardized ISO texture parameters [14]. The definitions, practical interpretations and measurements of 3D surface roughness parameters termed "areal surface texture" are presented by Leach [15]. The choice of the measurement (profiling) technique (stylus profilometer versus laser profilometer or atomic force microscope) depends on the scale of the surface roughness, i.e. from micro- to nano-scale [10, 14]. In this investigation, height parameters were analyzed in comparison to their computed values with a different scale of distortion shown in Fig. 4. In particular, a special searching algorithm which allows the selection of minimum and maximum values of *Rz* (*Rt*) parameter from 2, 3 or 10 surface profiles was implemented in order to consider the scattering of the measured data (see Fig. 5).

2.3 Computations of friction coefficient and elastic recovery

The friction coefficient for the rake face-chip contact can be determined as the ratio of the F_n (Eq. 3.3) and the F_m (Eq. 3.2) forces as follows:

$$\mu_\gamma = \frac{F_n}{F_m} = \frac{F_\gamma}{F_{\gamma N}} \tag{5}$$

where F_γ is the friction force and $F_{\gamma N}$ is the normal force on the rake face (Fig. 1b).

The elastic recovery of the machined surface corresponding to friction at the tool-chip interface defined by Eq. 5 is determined using the following equation [16, 17]:

$$\delta_s = r_n \left(1 - \frac{1+\mu_\gamma}{\sqrt{2\left(1+\mu_\gamma^2\right)}} \right) \tag{6}$$

where r_n is the measured cutting edge radius (Fig. 3b) and μ_γ is the friction coefficient on the rake face.

Equation (6) was derived based on the theory of elasticity applied to the case when an indenter of r_n radius loads an elastic half-space with defined friction coefficient [17, 18]. For this reason, the cutting edge radius was measured precisely (Fig. 3a) to determine accurate values of the elastic recovery (see Appendix Table 1).

Figure 2 shows that elastic recovery of the machined surface changes practically linearly with both the ploughing energy and friction coefficient μ_γ. It should be noted that PHT with the minimum feed of 0.025 mm/rev corresponds with the highest value of the friction coefficient equal to 2.5 and the specific ploughing energy of 43.1 GJ/m^3. In comparison, the corresponding value of the specific cutting energy in this case is equal to 17.6 GJ/m^3 which is in accordance with metal-cutting data [13, 19].

2.4 Computations of heights and smoothing rate of irregularities

The theoretical values of roughness height were determined using both the classical circle models (Eq. 7), expressing its correlation with the feed and the corner radius and more advanced elliptical model (known as the Brammertz's formula) which additionally considers the minimum UCT (h_{min} in Eq. 8) and in consequence a small unremoved area of the rough surface.

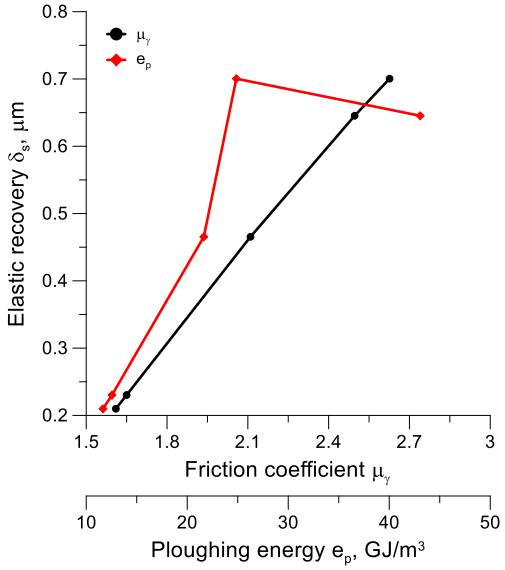

Fig. 2 Correlations between elastic recovery and ploughing energy and friction coefficient at the rake face

$$Rzt = \frac{f^2}{8r_\varepsilon} \tag{7}$$

$$Rzt^B = \frac{f^2}{8r_\varepsilon} + \frac{h_{\min}}{2}\left(1 + \frac{r_\varepsilon h_{\min}}{2}\right) \tag{8}$$

In this study, the smoothing effect resulting from the additional cut of irregularities during subsequent revolutions of the workpiece after their elastic recovery was taken into consideration. The appropriate formulas are as follows[19, 20]:

$$Rt_{\mathrm{sm}} = \frac{5f^2}{8r_\varepsilon} + \frac{h_{\min}}{2}\left(\frac{r_\varepsilon h_{\min}}{f^2} - 1\right) \tag{9a}$$

$$Rt'_{\mathrm{sm}} = \frac{4f^2}{8r_\varepsilon} + \frac{h_{\min}}{2}\left(1 + \frac{r_\varepsilon h_{\min}}{4f^2}\right) \tag{9b}$$

Equation 9a represents the case when the individual irregularity is re-generated after smoothing and Eq. 9b expresses the smoothing effect occurring in the second revolution of the workpiece. The second case takes place when the feed $f \leq \sqrt{r_\varepsilon h_{\min}}$ (for r_ε=0.8 mm and $h_{\min}$ = 0.8 μm, $f \leq$ 0.08 mm/rev). Equations 9a and 9b were derived by adding the first correction terms to Brammertz's formula given by Eq. 8 [20].

3 Experimental details

3.1 Workpiece material and cutting tool

The workpiece material was a 41Cr4 (AISI 5140 equivalent) alloy steel with Rockwell's hardness of 57 ± 1 HRC and initial *Sa* roughness of about 0.4 μm. In order to determine an accurate value of the minimum UCT, the cutting edge radius was determined using 3D image obtained on a focus variation microscope as shown in Fig. 3. It varies slightly in the range of 8–10 μm and, in consequence, computations for the elastic recovery (Eq. 6) were carried out assuming its lower and upper values of 8 and 10 μm. In Fig. 3b, a small land $b_\alpha \approx$ 6 μm can be noticed, so the smoothing effect can be expected as well. According to the well-established relation between the minimum UCT and the cutting edge radius, it was assumed that the ratio $h_{\min} = 0.1 r_n$ [3, 16, 19].

3.2 Hard turning conditions

Turning operations were performed on a CNC turning center, Okuma Genos L200E-M with an installed three-component Kistler dynamometer (model 9129A) and consumed energy-recording system. The resultant cutting force was resolved into three components—F_c, F_f and F_p. The measured signals were processed with a sampling rate of f = 1 kHz and a low-pass filter with a cut-off frequency of f_c = 300 Hz.

Initial finish hard turning (FHT) was performed with v_c = 150 m/min, f = 0.1 mm/rev, a_p = 0.15 mm and subsequent precision hard turning (PHT) operations with the same cutting speed but variable feed rate of 0.025, 0.035, 0.050, 0.060 and 0.075 mm/rev, respectively. CBN TNGA 160408 S01030 chamfered inserts with electro-erosion (ER) honed cutting edges. Typically, the cutting edge is prepared by sinking it into a counterface [21]. This special preparation technology allows to produce cutting edges with the minimum radius of about 5 μm. The cutting edge radius of r_n = 8–10 μm and chamfer width $b_\gamma \approx$100 μm were measured (see Fig. 3b). The cutting tool angles in the tool-in-hand system were the following: κ_r = 91°, λ_s = −6°, γ_{nc} = −30°, γ_n = −6°.

4 Experimental results and discussion

4.1 Factors influencing surface roughness in PHM

As pointed out in Section 1, surface generation in precision hard turning (PHT) is influenced by several distortion effects depending on the feed rate applied. They include such effects as elastic recovery caused by intensive ploughing action of the cutting edge, smoothing effect of the irregularities in subsequent revolutions and plastic side flow due to the lateral flow of the thermally softened material.

Values of measured and computed surface roughness parameters presented graphically in Fig. 4 are specified in Appendix Table 2.

In this study, all surface distortion effects are related to the maximum surface height *Sz* (surface topography) and corresponding 2D parameter *Rz* (surface profile).

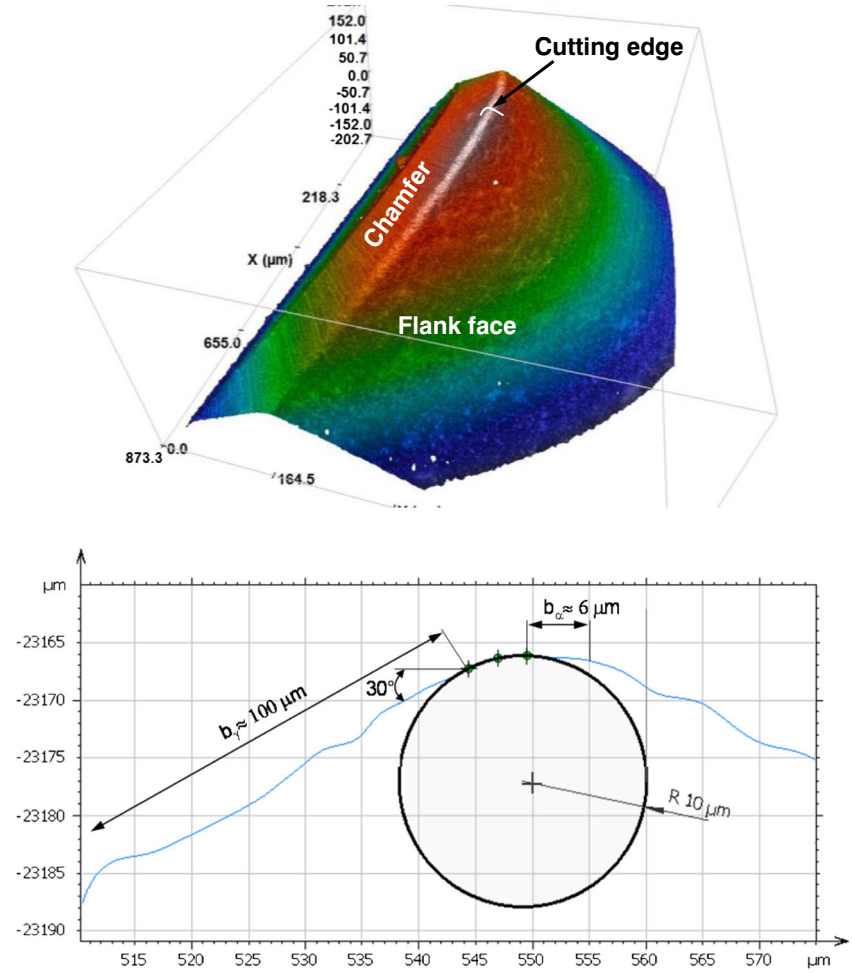

Fig. 3 Stereometric image of the cutting edge (**a**) and its dimensioning (**b**) at magnification ×200

According to Fig. 4, the elastic recovery modelled by Eq. 6 (curves #3a and 3b) was established to be mostly predominant at the minimum feeds of 0.025 and 0.035 mm/rev. This corresponds well with the Brammertz's model represented by curves #2a and 2b. It should be noted that springback effect seems to be important also when PHT with the feed rate higher than 0.06 mm/rev. The smoothing effect occurs simultaneously with the previous one and exists also at a higher feed up to about 0.05 mm/rev. When the feed exceeds 0.05 mm/rev, the Brammertz's model (Eq. 7) fits the measured *Sz* values better than the elastic recovery because it decreases as shown in Fig. 2. Finally, at the feeds between 0.075 and 0.1 mm/rev, surface profiles become more regular with a visible plastic flow effect at the highest feed (Fig. 6c, d). This observation is in a strong agreement with previous reports by Kishawy et al. [6]. All these influences were documented quantitatively by the introduction of appropriate analytical models.

In particular, in PHT the minimum value of *Rz* parameter is predicted with sufficient accuracy using theoretical formula,

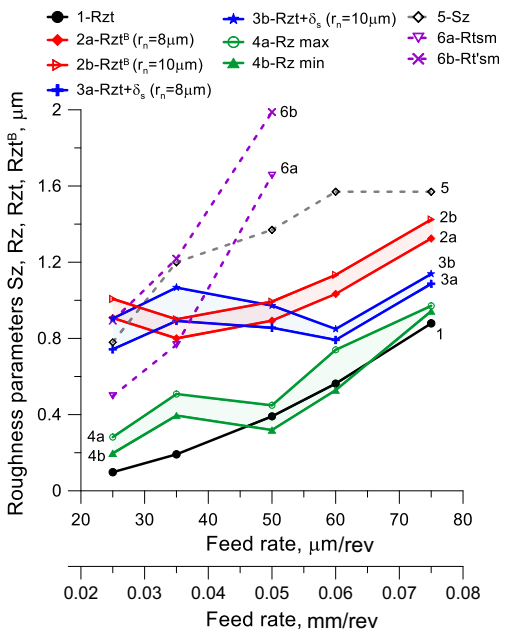

Fig. 4 Possible distortions influencing real surface roughness parameters 2D and 3D

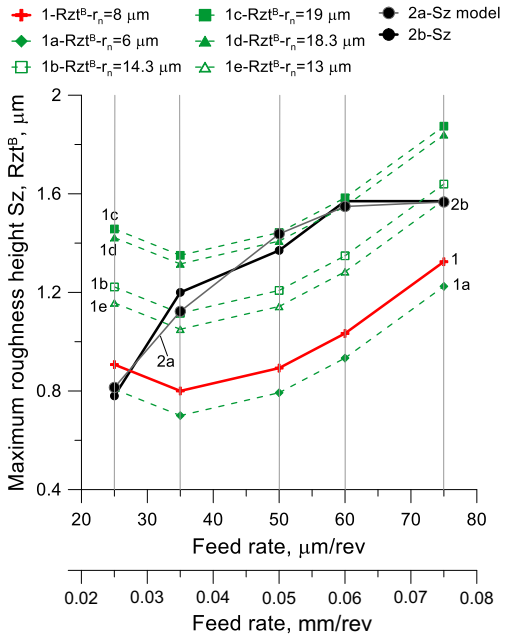

Fig. 5 Fitting of the predicted surface roughness parameter *Sz* to measured data predicted for: 1-r_n = 8 μm; 1a–r_n = 6 μm; 1b–r_n = 14.3 μm; 1c–r_n = 19 μm; 1d–r_n = 18.3 μm; 1e–r_n = 13 μm; 2a and 2b–predicted by Eq. 10/measured *Sz* parameter

but its maximum value needs the smoothing and springback effects to be considered (curves #4a and 4b). In contrast, the *Sz* value is closer to the Brammertz's formula or more accurately to the smoothing effect at the minimum feeds applied.

Figure 5 shows the graphical method for fitting the predicted values of the maximum roughness height to the measured values of *Sz* parameter (curve #2b). In the first step, the model of the function *Sz* = f (*f*) (curve #2a) was determined using polynomial model in the form of

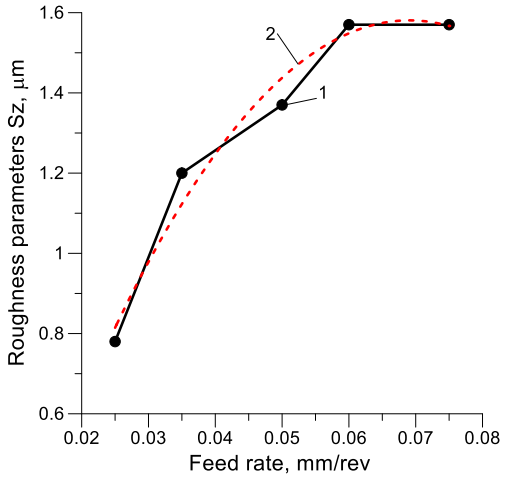

Fig. 6 Graphical interpretation of Eq. 10. Measured (1) and predicted (2) values of Sz parameter defined in ISO 25178 as the maximum height of the surface

$$\mathrm{Sz} = -0.3023 + 54.545f - 394.97f \tag{10}$$

and using this model, the values of cutting edge radii were computed for all the values of feed rate (0.025, 0.035, 0.050, 0.060 and 0.075 mm/rev) and constant tool nose radius of 800 μm. In case of empirical Eq. 10, the R-squared is equal to R^2 = 0.9718 and the residual sum of squares is equal to 0.0122. It was found that the relevant values of the cutting edge radius which satisfy Eq. 10 are equal to 6, 14.3, 19 and 13 μm, respectively. On the other hand, the next possibility is to change the tool nose radius, i.e. decrease it for lower feeds and increase it for higher feeds.

The measured values and values of the maximum height of the surface Sz predicted by Eq. 10 are presented separately in Fig.6.

4.2 Analysis of surface topography in terms of constitutive conditions

Figure 7 shows a series of zoomed surface topographies recorded by means of a confocal 3D profilometer showing characteristic distortion modes obtained at feed rates of 0.025, 0.050 and 0.075 mm/rev and additionally, a reference surface topography with regular feed marks generated at the feed of 0.1 mm/rev. Representative surface textures obtained in PHT operations are labelled by the measured values of 3D roughness parameters. The measured values of *Sa* and *Sz* parameters range from 0.07 to 0.21 μm and 0.2 to 1.6 μm, respectively.

The minimum and maximum values of *Rz* (Fig. 4) determined from two and three automatically selected profiles varied between 0.22–0.95 μm and 0.28–0.97 μm, respectively. The regular distribution of feed mark characteristic for CBN turned surface with feed rate of 0.1 mm/rev is visualized in Fig. 7d. In Fig. 7d also, regular material pile-ups at the secondary cutting (trailing) edge caused by material side flow can be observed. This effect corresponds well quantitatively with FEM predictions made by Kishawy et al. [6] and Schaal et al. [7]. For sharp tools, the maximum springback in metal cutting is equal to δ_s = 0.3–1.6 μm.

It should be emphasized that plastic side flow results from lateral plastic flow of the material locally heated up to 900–1000 °C [22]. In addition, associated abrasive wear of the cutting tool is more likely than adhesion [23].

In this study for precision machining it ranges from 0.2 to 0.8 μm depending on the ploughing intensity (Fig. 2). On the other hand, the height of lateral flashes resulting from the material side flow which develops at

a f=25 μm, Rt= 0.31 μm, Rz= 0.28 μm, St/Sz= 0.78 μm

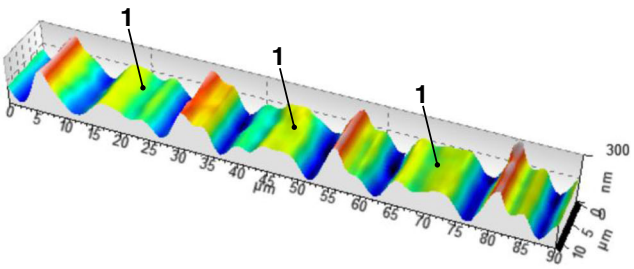

b f=50 μm, Rt=0.52 μm, Rz= 0.45 μm, St/Sz= 1.37 μm

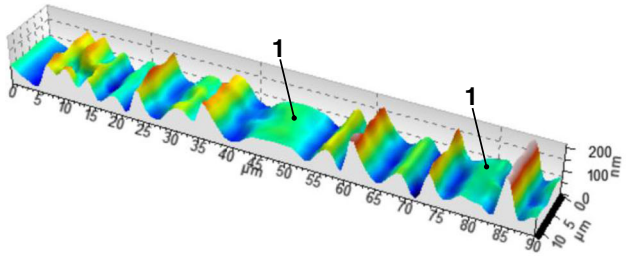

c *f*=0.075 mm/rev, *Rt*=0.97 μm, *Rz*= 0.97 μm, *St/Sz* = 1.57 μm

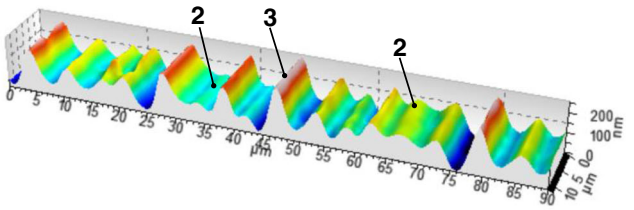

d *f*=0.1 mm/rev, *Rt*=1.19 μm, *Rz*=1.13μm, *St/Sz*=2.84 μm

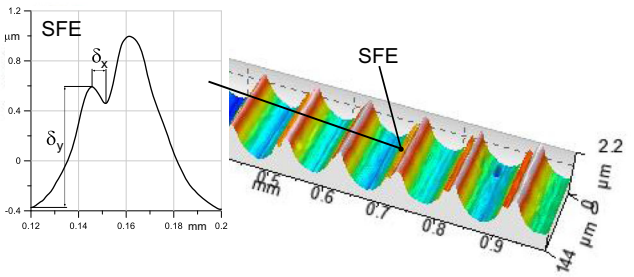

Fig. 7 Characteristic surface topographies obtained at different feeds. **a** 0.025 mm/rev. **b** 0.05 mm/rev. **c** 0.075 mm/rev. **d** 0.1 mm/rev. Cutting speed v_c = 150 m/min, depth of cut a_p = 0.03–0.15 mm. One and two fully and partially smoothed peaks, three full peaks, SFE side flow effect. Magnification ×200

feed of 0.1 mm/rev is about δ_y = 1 μm as denoted in Fig. 7d. Moreover, the corresponding average nodal displacement is about δ_x = 5 μm which coincides with computed data in Ref. [6]. The regular feed marks produced in hard turning operations using low and high feed rates are visualized in Fig. 8. In general, the measured distances between feed marks are practically equal to the nominal values of feed rates selected in this study.

5 Conclusions

1. In precision, hard turning performed with CBN cutting tools and feed rate of 0.025–0.075 mm/rev such surface distortion effects as elastic recovery (springback) caused by an intensive ploughing action of the cutting edge, smoothing effect of the generated irregularities in subsequent revolutions and plastic side flow resulting from lateral plastic flow are revealed depending on the feed rate applied.

2. The elastic recovery was established to be mostly predominant at the minimum feeds of 0.025 and 0.035 mm/rev. The smoothing effect occurring simultaneously with the elastic recovery is also extended to a higher feed of 0.050 mm/rev.

3. At the feeds of 0.075 μm and 0.1 mm/rev the minimum uncut chip thickness increases and both these phenomena weaken visibly while surface profiles (topographies) become more regular. Additionally, visible flashes of about 0.6 μm in height caused by the side flow effect appear.

4. The three effects were documented quantitatively by the introduction of appropriate analytical models. In particular, in PHT the minimum value of *Rz* parameter is predicted with sufficient accuracy using theoretical formula but its maximum value needs the cutting edge sharpness to be considered. In contrast, the *Sz* values are closer to the Brammertz's formula or more accurately to smoothing effect at the minimum feed rates applied.

5. An original graphical method for fitting the predicted and measured values of the maximum surface height by searching the correct values of the cutting edge radius is proposed. As a result, an empirical model for prediction of

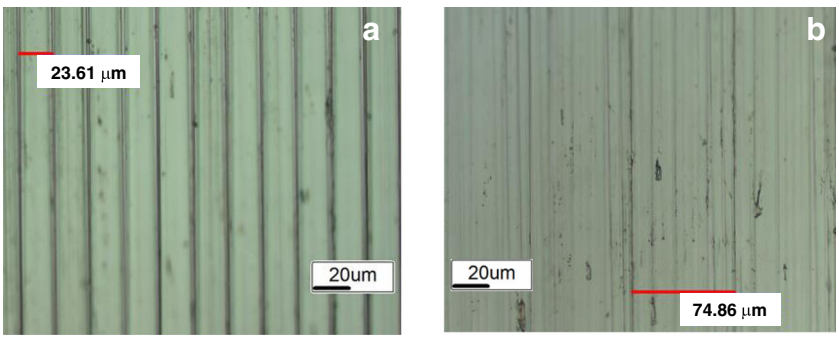

Fig. 8 Optical images of surface topographies obtained at low (**a**) 0.025 mm/rev and high (**b**) 0.075 mm/rev feeds at magnification ×200

the Sz parameter in terms of the feed rate used is derived. Moreover, the possible distortions of the machined surface topographies are visualized in the form of isometric views.

6. Future trends can be focussed on experimental investigations in micro-scale using specially designed devices and accurate FEM-based modelling of surface generation mechanisms including associated distortion effects. It is also important to design cutting tools with precisely prepared cutting edges, keeping the recommended cutting edge radius and the tool corner radius. It is also plausible to extend this analysis to higher tool corner radiuses, i.e. 1.2, 1.6 or 2.4 mm.

Nomenclature

a_p	depth of cut
b_γ	chamfer width
b_α	land width at the flank face
e_c	specific cutting energy
e_p	specific ploughing energy
f	feed rate
h_{min}	minimum uncut chip thickness
h_m	average uncut chip thickness
l_k	length of the equivalent cutting edge
r_n	radius of the cutting edge
r_ε	radius of tool corner
v_c	cutting speed
A_c	cross-sectional area of cut
F_c	cutting force
F_f	feed force
F_p	passive force
F_l	force parallel to the cutting edge
F_m	force perpendicular to the rake face
F_n	force parallel to the rake face
F_γ	friction force
$F_{\gamma N}$	normal force on the rake face
Ra	average value of surface roughness
Rz	maximum roughness height
Rzt	theoretical value of Rz parameter
Rzt^B	theoretical value of Rz parameter predicted by Brammertz's model
Sa	arithmetic mean height of the surface
Sz	ten point height of the surface
St	total height of the surface
γ_n	normal rake angle
γ_{nc}	chamfer angle
λ_s	tool inclination angle
μ_γ	friction coefficient at the rake face
δ_s	springback value
δ_x	nodal displacement of the peak
δ_y	height of a pile-up

Abbreviations

CBN	cubic boron nitride
FEM	finite element method
HPT	high precision turning
PCD	polycrystalline diamond
HPM	high precision machining
SFE	side flow effect
TM	transformation matrix
UCT	uncut chip thickness

Appendix

Table 1 Values of cutting forces, specific ploughing energy, friction coefficient and elastic recovery

Feed, f (mm/rev)	Force F_c (F_z) N	Force F_p (F_y) N	Force F_f (F_x) N	Specific energy e_p (GJ/m^3)	Friction coefficient $\mu_{\gamma n}$	Elastic recovery δ_s (r_n = 8 μm) (μm)	Elastic recovery δ_s (r_n = 10 μm) (μm)
0.025	13.20	32.30	3.70	24.86	2.63	0.70	0.81
0.035	17.10	43.50	8.00	43.07	2.50	0.65	0.88
0.05	26.00	54.10	9.90	21.64	2.11	0.47	0.58
0.06	64.90	113.00	36.40	12.56	1.65	0.23	0.29
0.075	77.20	131.20	41.80	11.66	1.61	0.21	0.26

Table 2 Values of measured and computed surface roughness parameters

Feed, f (mm/rev)	Sa (μm)	Ra, (μm)	Sz (μm)	Rz_{max}, (μm)	Rz_{min}, (μm)	R_{zt} (μm)	R_t^B (μm)
0.025	0.07	0.04	0.78	0.282	0.197	0.10	1.01
0.035	0.138	0.065	1.20	0.508	0.395	0.19	0.90
0.05	0.14	0.07	1.37	0.449	0.319	0.39	0.99
0.06	0.21	0.13	1.57	0.740	0.528	0.56	1.13
0.075	0.28	0.26	1.57	0.971	0.943	0.88	1.42

References

1. Davim JP (ed) (2011) Machining of hard materials. Springer, Berlin
2. Grzesik W (2017) Advanced machining processes of metallic materials. Elsevier, Amsterdam
3. Grzesik W (1996) A revised model for predicting surface roughness in turning. Wear 194:143–148
4. Knueferman MMW, McKeown PA (2004) A model for surface roughness in ultraprecision hard turning. Ann CIRP 53:99–102
5. Childs THC, Sekiya K, Tezuka R, Yamane Y, Dornfeld D, Lee DE, Min S, Wright PK (2008) Surface finishes from turning and facing with round nosed tools. Ann CIRP Manuf Technol 57:89–92
6. Kishawy HA, Haglund A, Balazinski M (2006) Modelling of material side flow in hard turning. Ann CIRP Manuf Technol 55:85–88
7. Chen T, Qiu C, Liu X (2017) Study on 3D topography of machined surface in high-speed hard cutting with PCBN tool. Int J Adv Manuf Technol 91:2125–2133
8. Schaal N, Kuster F, Wegener K (2015) Springback in metal cutting with high cutting speeds. Proc CIRP 31:24–28
9. Benardos PG, Vosniakos G-C (2003) Predicting surface roughness in machining: a review. Int J Mach Tools Manuf 43:833–844
10. Jiang XJ, Whitehouse DJ (2012) Technological shifts in surface metrology. Ann CIRP Manuf Technol 61:815–836
11. Ozel T, Hsu T-K, Zeren E (2005) Effects of cutting geometry, workpiece hardness, feed rate and cutting speed on the surface roughness and forces in finish turning of hardened AISI H13 steel. Int J Adv Manuf Technol 25:262–269
12. Grzesik W, Rech J, Żak K (2014) Determination of friction in metal cutting with tool wear and flank face effects. Wear 317:8–16
13. Grzesik W, Denkena B, Żak K, Grove T, Bergman B (2015) Energy consumption characterization in precision hard machining using CBN cutting tools. Int J Adv Manuf Technol 85:2839–2845
14. Pawlus P, Wieczorowski M, Mathia T (2014) The errors of stylus methods in surface topography measurements. Zapol Publ, Szczecin
15. Leach R (ed) (2013) Characterisation of areal surface texture. Springer, Berlin
16. W. Grzesik (2010) Generation and modelling of surface roughness in machining using geometrically defined cutting tools. In: Metal cutting. Research Advances, Nova Science Publishers, Chapter 6, New York 163–185
17. Zheleznov GS, Singeev SA (1983) Calculation of forces acting on the tool flank face (in Russian). Izvestija VUZ Mashinostroenie 9: 146–148
18. Yuan ZJ, Zhou M, Dong S (1996) Effects of diamond tool sharpness on the minimum cutting thickness and cutting surface integrity in ultraprecision machining. J Mat Proc Technol 62:327–330
19. Grzesik W (2010) Fundamentals of machining of construction materials. WNT (in Polish), Warsaw
20. Miko E (2005) Generation of micro-irregularities on metallic surfaces machined with cutting tools with defined geometry (in Polish), Scientific Monograph No. 46. Publishing House of Kielce University of Technology, Kielce
21. Denkena B, Biermann D (2014) Cutting edge geometries. Ann CIRP Manuf Technol 63:631–653
22. Wang JY, Liu CR (1999) The effect of tool flank wear on the heat transfer, thermal damage and cutting mechanics in finish hard turning. Ann CIRP 48:53–58
23. Chinchanikar S, Choudhury SK (2015) Machining of hardened steel-experimental investigations, performance modelling and cooling techniques: a review. Int J Mach Tools Manuf 89:95–109